

Lightweight Node Selection in Hexagonal Grid Topology for TDoA-Based UAV Localization

Zexin Fang*, Bin Han*, Wenwen Chen*, and Hans D. Schotten*[†]

*University of Kaiserslautern-Landau (RPTU), Germany

[†]German Research Center for Artificial Intelligence (DFKI), Germany

Abstract—This paper investigates the optimization problem for Time Difference of Arrival (TDoA)-based unmanned aerial vehicle (UAV) localization in low-altitude urban environments with hexagonal grid node deployment. We derive a lightweight optimized node selection strategy based on only received signal strength (RSS) measurements, to pre-select optimal nodes, avoiding extensive TDoA measurements in energy-constrained UAV scenarios. Theoretical and simulation results demonstrate that dynamically selecting the number of reference nodes improves localization performance while minimizing resource overhead.

Index Terms—UAV; TDoA; localization.

I. INTRODUCTION

The Low Altitude Economy (LAE) represents an emerging economic sector that leverages low-altitude airspace for commercial and social aviation operations. It includes diverse types of aircraft conducting missions in areas such as transportation, logistics, tourism, agriculture, and disaster monitoring [1]. As low-altitude airspace becomes increasingly utilized for diverse flight activities, accurate localization, particularly for unmanned aerial vehicles (UAVs), grows critical for effective task execution and collision avoidance, especially when Global Navigation Satellite System (GNSS) proves unreliable.

Current high-accuracy UAV localization solutions include: *i*) computer-vision based solution; *ii*) sensing based solution; *iii*) Radio Frequency (RF) based self-localization. Computer-vision based solutions offer flexibility [2] but face daytime and legal constraints, such as General Data Protection Regulation (GDPR) in Germany. Sensing-based solutions provide high-accuracy localization by sharing position information, removing computational burden from the aircraft. However, both approaches introduce latency due to heavy computational requirements and are highly distance-sensitive, therefore limiting applications for high-mobility UAVs. Compared to these solutions, RF based self-localization is lightweight and universally applicable. It captures parameters from multiple references, such as received signal strength (RSS), Time Difference of Arrival (TDoA), or Direction of Arrival (DoA), and combines these measurements with reference positions for self-localization. TDoA-based methods are commonly preferred due to their simpler implementation compared to DoA-based methods and higher accuracy than RSS-based methods [3].

Most existing research assumes dedicated sensor networks with synchronized nodes to support accurate localization. Recent work has addressed energy-efficient node selection [4]–[6], often focusing on classifying nodes by Non-Line-of-Sight

(NLOS) and Line of Sight (LOS) conditions. However, less attention has been given to the deployment topology of these sensors in practical scenarios. While the Cramer-Rao bound (CRB) indicates that localization accuracy improves with more sensor nodes, this is constrained by sensor deployment in practice. Without comprehensive link adaptation, including distant nodes may degrade accuracy due to unreliable TDoA measurements. Therefore, inspired by previous research, we investigate the impact of node deployment on localization accuracy. We consider a hexagonal grid topology for reference node placement based on two considerations. First, hexagonal grids provide uniform coverage for practical wireless deployments. Second, with Sixth Generation (6G) networks, base stations are becoming smaller and more densely deployed, making high-accuracy TDoA-based localization increasingly feasible. While fewer works focus on base station-based TDoA localization, with synchronization being the primary challenge [7]–[9], embedding localization nodes within base station infrastructure is compelling as it requires no additional deployment.

In Sec.II, we investigate the Air to Ground (A2G) model to provide a foundation for subsequent optimization analysis. In Sec.III, we introduce the CRB of TDoA measurement, formulate the objective function for self-localization optimization, and analyze this optimization problem theoretically. In Sec.IV, we introduce an algorithm to find optimal node selection using only RSS, avoiding unnecessary TDoA measurements to reduce localization latency. We validate our optimization framework and algorithm in Sec.V and conclude in Sec. VI.

II. CHANNEL MODELING

The A2G channel characteristics were extensively investigated by 3rd Generation Partnership Project (3GPP) in [10]. In the Urban Micro-Aerial Vehicle (UMi-AV) channel model, the probability of LOS is described with:

$$P_{\text{los}} = \begin{cases} 1, & d_{2D} \leq d_1; \\ \left(1 - \frac{d_1}{d_{2D}}\right) \exp\left(\frac{-d_{2D}}{p_1}\right) + \frac{d_1}{d_{2D}}, & d_{2D} > d_1. \end{cases} \quad (1)$$

Where d_{2D} represents the horizontal distance between the aerial vehicle and the ground base station, and h denotes the height. Meanwhile, d_1 and p_1 are defined as:

$$\begin{aligned} d_1 &= \max(294.05 \log_{10}(h) - 432.94, 18); \\ p_1 &= 233.98 \log_{10}(h) - 0.95. \end{aligned} \quad (2)$$

Summarizing LOS and NLOS conditions, the average path loss component can be described with,

$$\eta = (4.32 - 0.76 \log_{10}(h))(1 - P_{\text{los}}) + (2.225 - 0.05 \log_{10}(h))P_{\text{los}} \quad (3)$$

When $d_{2D} \leq d_1$, the channel is dominated by LOS, which we define as area 1 (A1). Conversely, when $d_{2D} > d_1$, the channel can be either LOS or NLOS depending on the distance and height; consequently, we designate this region as area 2 (A2). We then formulated the average η in Eq. (4), the first derivative of η with respect to d_{2D} in Eq. (5), and the second derivative in Eq. (6), respectively.

$$\eta = \begin{cases} 2.225 - 0.05 \log_{10} h, & \text{if in A1;} \\ (4.32 - 0.76 \log_{10}(h))(1 - P_{\text{los}}) + (2.225 - 0.05 \log_{10}(h))P_{\text{los}}, & \text{if in A2.} \end{cases} \quad (4)$$

$$\eta' = \begin{cases} 0, & \text{if in A1;} \\ \underbrace{\left(0.71 \log_{10}(h) - 2.07\right)}_{<0} \underbrace{\left(\left[-\frac{d_1}{d_{2D}^2} - \frac{1 - \frac{d_1}{d_{2D}}}{p_1}\right]\right)}_{<0} & \text{if in A2.} \\ \underbrace{\exp\left(-\frac{d_{2D}}{p_1}\right)}_{>0} - \underbrace{\frac{d_1}{d_{2D}^2}}_{>0} & \end{cases} \quad (5)$$

$$\eta'' = \begin{cases} 0, & \text{if in A1;} \\ \underbrace{\left(0.71 \log_{10}(h) - 2.07\right)}_{<0} \underbrace{\left(\left[\frac{2d_1}{d_{2D}^3} + \frac{d_{2D} - d_1}{p_1^2 d_{2D}}\right]\right)}_{>0} & \text{if in A2.} \\ \underbrace{\exp\left(-\frac{d_{2D}}{p_1}\right)}_{>0} + \underbrace{\frac{2d_1}{d_{2D}^3}}_{>0} & \end{cases} \quad (6)$$

Considering the practical constraints, the UAV must fly above a minimum height to avoid collisions in urban areas while remaining below a maximum height to comply with legal regulations [11], we have:

$$C1 : h \in [20, 120]. \quad (7)$$

Under constraint C1, we observe that $0.71 \log_{10}(h) - 2.07 < 0$, therefore both $\eta' \geq 0$ and $\eta'' \leq 0$ hold. This indicates that η is monotonically increasing with diminishing rate. The averaged values of η are presented in Fig. 1. It should be noted that the A2G model, according to the definition in [10], is only applicable when $h \geq 22.5$ m. Below 22.5 m, a different model from [12] should be applied. However, to simplify our analysis, we extended the A2G model down to 20 m.

III. PROBLEM FORMULATION

A. Objective equivalence

CRB of three dimensional (3D) localization can be described as a formula of the modeled distance error σ_M and the number of reference nodes N ,

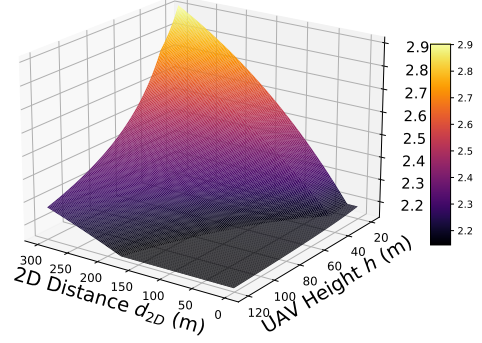


Fig. 1: Path loss component η with respect to d_{2D} and h (A1 is the black plane and A2 is the curved surface)

$$\sigma_\theta^2 \geq \frac{6\sigma_M^2}{N} \quad (8)$$

Eq. (8) is derived under the assumption that all reference nodes are uniformly distributed around the UAV, with numerical validation provided in [13]. While σ_M comprises both position error variance σ_p and distance error variance σ_d , we can simplify our analysis by considering static references as reliable. Despite neglecting σ_p , σ_M remains mathematically intractable. Therefore, we simplify it to a tractable approximation:

$$\sigma_\theta^2 \propto \frac{1}{N} \left(\frac{\sum_{n=1}^N \sigma_{n,d}}{N} \right)^2, \quad (9)$$

where $\sigma_{n,d}$ denotes the distance error variance for individual communication links with nodes. According to [14], [15], under dense multi-path scenario the CRB for TDoA measurements is $\sigma_d^2 \geq J_T^{-1}$, where J_T represents the Fisher information for TDoA estimation, with

$$J_T = 2c^{-1}4\pi^2 \text{SINR} \gamma \beta^2 \sin^2(\phi). \quad (10)$$

where c is the speed of light and SINR denotes the Signal to Interference and Noise Ratio (SINR), with interference primarily due to multipath effects. Since the UAV's subchannels have closely spaced carrier frequencies in a dense urban environment, their multipath profiles are highly correlated and vary predominantly with altitude. Thus, we model $\text{SINR} = \text{SNR} \cdot R$, where R represents an interference-to-noise ratio factor treated as constant across links to simplify analysis. Meanwhile, the parameters γ and $\sin^2(\phi)$ represent the whitening gain and information loss due to path loss nuisance parameters, respectively. As demonstrated in [16], while both γ and $\sin^2(\phi)$ vary with β , the variation in $\sin^2(\phi)$ is negligible compared to that of γ . Consequently, J_T is predominantly scaled by SNR, β , and γ . The whitening gain γ can be characterized with,

$$\gamma = \frac{\text{SNR}_w}{\text{SNR}} = \frac{P_{\text{wpre}}}{P_{\text{wpost}}}$$

$$P_{\text{wpre}} = \int_{-\frac{\beta}{2}}^{\frac{\beta}{2}} s_n(f) df; \quad P_{\text{wpost}} = S_n^w \beta.$$

Where P_{wpre} and P_{wpost} denote the noise power before and after the whitening process, After whitening, the PSD of noise become flat, denoted as S_n^w . Consider $s_n(f)$ to be modeled with power-law noise model $s_n(f) = Cf^{-\alpha}$. Then we can have,

$$P_{\text{wpre}} = \int_{-\frac{\beta}{2}}^{\frac{\beta}{2}} Cf^{-\alpha} df = 2\alpha C \ln\left(\frac{\beta}{2}\right).$$

Considering $\alpha = 1$ is common in real-world systems, therefore,

$$\gamma = \frac{P_{\text{wpre}}}{P_{\text{wpost}}} = \frac{2C \ln\left(\frac{\beta}{2}\right)}{S_n^w \beta},$$

we can further simplify this to $\gamma \propto \ln(\beta)\beta^{-1}$, since β is the bandwidth, typically $\ln(\beta) \gg \ln(2)$. The channel between UAVs and ground infrastructures can be modeled as a Rician channel. The K factor also influences many aforementioned factors in Eq. (10). In urban environments, the K factor typically exhibits limited variation subjected to the altitude; therefore, subsuming γ into Eq. (10), we reasonably assume that $\sigma_{n,d}^2$ is primarily governed by two factors, with the proportional relationship: $\sigma_{n,d}^2 \propto (\text{SNR}_n \beta_n \ln \beta_n)^{-1}$. Considering that in practice, transmitting power is usually proportional to bandwidth, and so is the noise floor,

$$P_n = \psi \beta_n, \quad N_n = N_0 \beta_n, \quad (11)$$

where ψ is the transmitting power spectral density and N_0 is the noise power spectral density, respectively. Since sub-band bandwidths are typically much smaller than the central carrier frequency, differences in carrier frequency can be neglected. Under these assumptions, the proportion $\text{SNR}_n \propto d_{3D,n}^{-\eta_n}$ holds. With $\sigma_n^2 \propto d_{3D,n}^{\eta_n} (\beta_n \ln \beta_n)^{-1}$, substituting this into Eq. (9):

$$\sigma_\theta^2 \propto N^{-3} \left(\sum_{n=1}^N d_{3D,n}^{\frac{1}{2}\eta_n} (\beta_n \ln \beta_n)^{-\frac{1}{2}} \right)^2. \quad (12)$$

B. Reference deployment

When an UAV is flying above a dense urban area, it is reasonable to assume that reference nodes from different directions are available. In such cases, the UAV can select the nearest reference nodes to optimize its self-localization performance. Therefore, the d_{2D} to N_{th} nearest node can be described as a monotonically increasing function $d_{2D}(N)$. For

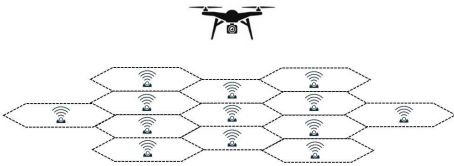


Fig. 2: system model

a hexagonal grid topology for reference deployment, depicted in Fig. 2. $d_{2D}(N)$ is:

$$d_{2D}(N) \begin{cases} = \Delta, & \text{if } N = 1, \\ \in [R - \Delta, R + \Delta], & \text{if } 1 < N \leq 7, \\ \vdots \\ \in [kR - \Delta, kR + \Delta], \\ \text{if } 3k^2 - 3k + 1 < N \leq 3k^2 + 3k + 1, \end{cases} \quad (13)$$

where Δ is the distance to the 1st reference node, R is the coverage of reference nodes, and $\Delta \in [0, R/2]$. k is the layer of the hexagonal grids. Apparently, $d_{2D}(N)$ is a piecewise function; however, we can still summarize its derivative segmentwise as,

$$d'_{2D}(N) \begin{cases} = \Delta, & N = 1, \\ \approx \frac{\Delta}{3}, & 1 < N \leq 7, \\ \vdots \\ \approx \frac{\Delta}{3k}, & 3k^2 - 3k + 1 < N \leq 3k^2 + 3k + 1. \end{cases} \quad (14)$$

We can conclude that, $d'_{2D}(N) > 0$ and $d''_{2D}(N) \approx 0$ in most cases, with averaged values of 5000 numerical simulation depicted in Fig. 3.

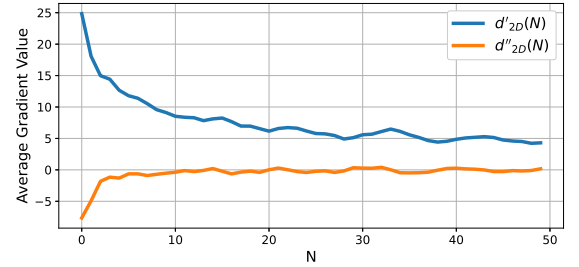


Fig. 3: $d'_{2D}(N)$ and $d''_{2D}(N)$ when $R = 120$ m

C. Localization optimization

In multi-UAV systems sharing ground infrastructure, sub-band bandwidth can be fixed and pre-determined for efficient multiplexing. We analyze localization performance when β_n remains constant, where each UAV optimizes its own localization accuracy based on available information. Consequently, Eq. (12) can be further simplified as following,

$$\sigma_\theta^2 \propto N^{-3} \left(\sum_{n=1}^N d_{3D,n}^{\frac{1}{2}\eta_n} \right)^2, \quad (15)$$

$$\sum_{n=1}^N d_{3D,n}^{\frac{1}{2}\eta_n} = \sum_{n=1}^N (d_{2D,n}^2 + h^2)^{\frac{1}{4}\eta(d_{2D,n}, h)}, \quad (16)$$

$$\Phi(N) = \sum_{n=1}^N (d_{2D,n}^2 + h^2)^{\frac{1}{4}\eta(d_{2D,n}, h)}, \quad (17)$$

$$\phi(N) = (d_{2D,n}^2 + h^2)^{\frac{1}{4}\eta(d_{2D,n}, h)}, \quad (18)$$

and referring Eq. (15), we formulate the optimization problem:

$$\begin{aligned} \min_N \quad & F_\theta(N) = \Phi^2(N)N^{-3} \\ \text{s. t. :} \quad & N \in \mathbb{Z}_{>1}, \\ & h \in \mathbb{R}^+, \\ & d_{2D,n} \in \mathbb{R}^+, \quad d_{2D,n} \geq \Delta, \quad n \in \mathcal{N}. \end{aligned} \quad (19)$$

$\Phi(N)$ is discrete sum function and can be approximated by continuous function by applying the Euler–Maclaurin summation formula:

$$\Phi(N) \approx \int_1^N \phi(x) dx + \frac{\phi(N)}{2} + \frac{\phi'(N)}{12} - \frac{\phi'''(N)}{720} + \dots \quad (20)$$

Correspondingly, $\Phi'(N)$ takes the form,

$$\Phi'(N) \approx \phi(N) + \frac{\phi'(N)}{2} + \frac{\phi'''(N)}{12} - \frac{\phi''''(N)}{720} + \dots \quad (21)$$

The first-order derivative and the second-order derivative of $\phi(N)$ are given in Eqs. (23)–(24). Recalling Eqs. (4)–(6), our numerical results indicate mean values for η , η' , and η'' of 2.3, 4.8×10^{-3} , and 2.1×10^{-5} , respectively. We can conclude that $\phi(N) \gg \frac{\phi'(N)}{2} \gg \frac{\phi''(N)}{12}$. To simplify our analysis, we take:

$$\Phi'(N) \approx \phi(N) + \frac{\phi'(N)}{2} \quad (22)$$

Meanwhile, the first-order derivative and the second-order derivative of $F_\theta(N)$ are given in Eqs. (25)–(26). With the given information, we cannot determine the monotonicity of $F_\theta(N)$. Furthermore, the sign of $F_\theta''(N)$ is difficult to determine since both positive and negative terms are involved. However, we can write $F_\theta'(N)$ in the form:

$$F_\theta'(N) = \underbrace{2N^{-3}\Phi(N)}_{T_1(N)} \underbrace{\left(\phi(N) - \frac{3}{2N}\Phi(N) + \frac{\phi'(N)}{2} \right)}_{T_2(N)}, \quad (27)$$

$$\frac{\partial T_2(N)}{\partial N} = \left(\frac{2N-3}{2N} \right) \phi'(N) + \frac{3}{2N^2} \phi(N) + \frac{1}{2} \phi''(N). \quad (28)$$

Within Eq. (27), clearly $T_1(N) > 0$, and the sign of $T_2(N)$ can't be determined. Consequently, $\frac{\partial T_2(N)}{\partial N}$ is given in Eq. (28). In this equation, while $N \geq 2$, $\frac{\partial T_2(N)}{\partial N} \geq 0$ always holds; in the case $N = 1$, we still have $\frac{3\phi(N)}{2} > \frac{\phi'(N)}{2}$. Therefore, $\frac{\partial T_2(N)}{\partial N} > 0$ always holds, indicating that T_2 is monotonically increasing. When $N = 1$, $T_2(N) = -\frac{\phi(N)}{2} + \frac{\phi'(N)}{2}$. With $\phi(N) \gg \phi'(N)$ and $\lim_{N \rightarrow \infty} T_2(N) > 0$, we can conclude that $T_2(N)$ is not only monotonically increasing, but also increasing from a negative value to a positive value. In summary of all analysis, despite the lack of convexity proof for $F_\theta(N)$, at the point where $T_2(N) = 0$, its left side satisfies $F'(\theta) < 0$ and its right side satisfies $F'(\theta) > 0$, therefore an optimal solution exists.

IV. PROPOSED METHOD

Facilitating the average A2G channel statistics, previous analysis demonstrated an optimal node selection number N_{opt} exists. However, in practice, η of different links cannot be obtained without extensive channel estimation. Meanwhile, accessing $d_{2D}(N)$ is challenging since ranging methods are error-prone, and using TDoA for all communication links is computationally expensive and introduces latency. Since precisely solving N_{opt} introduces significant complexity, we propose a lightweight approach using only RSS, offering advantages: *i*) extremely lightweight, requiring no additional processing; *ii*) nodes with poor channels are automatically excluded due to significantly large estimated distances; *iii*) sensitive to LOS probability mismatch caused by environmental factors in A2G models, enabling possible compensation. The detailed algorithm is introduced in Alg. 1.

After assessing the optimal strategy for localization, TDoA of selected nodes will be measured, we then employ the gradient algorithm presented in [17] for localization. This algorithm is superior to other localization algorithms in scenarios where the reference positions exhibit limited dynamic range in altitude.

Algorithm 1: RSSI-based optimum finder

```

1 Input: estimated distances based on RSS  $d_n^R$ ; altitude  $h$ ; averaged path loss
   component consolidated as a table  $\bar{\eta}(d_{2D}, h)$ ; maximum reference numbers
    $N_m$ 
2 Function :
3   sort  $d_n^R$ ;
4   for  $n = 1 : N_m$  do
5      $d_{2D,n} = \sqrt{(d_n^R)^2 - h^2}$ 
6     find  $\bar{\eta}$  regarding  $d_{2D,n}$  and  $h$ 
7     compute  $\phi_n$  referring Eq. (18)
8   compute  $\Phi_n$  referring Eq. (17)
9   compute  $T_{2,n}$  referring Eq. (27)
10   $T_2 \leftarrow \{T_{2,n}; n \in [1, N_m]\}$ 
11   $N_{\text{opt}} \leftarrow |\{n \in [1, N_m] : T_2[n] < 0\}|$  // Count the number
   of negative values
12  if  $\bar{T}_2 > 0$  then
13     $T_2^\circ = T_2 - \bar{T}_2$ 
14  else
15     $T_2^\circ = T_2 + |\bar{T}_2|$  // compensate for  $\eta$  miss-match
16   $N_{\text{opt}}^\circ \leftarrow |\{n \in [1, N_m] : T_2^\circ[n] < 0\}|$ 
17   $N_{\text{opt}} = \text{round}(\frac{N_{\text{opt}}}{2} + \frac{N_{\text{opt}}^\circ}{2})$ 
18   $N_{\text{opt}} = \min(20, \max(N_{\text{opt}}, 3))$  // set upper and lower
   boundaries

```

V. SIMULATION RESULTS

In this section, we validate the performance of Alg. 1 under different deployment configurations of reference nodes and varying altitudes of the UAV. We assume the UAV is positioned in the relative center of the area with reference nodes evenly distributed from all directions, eliminating unilateral reference problems. All sensor nodes are synchronized and periodically broadcast equal-powered reference signals containing their positions and TDoA information. The detailed simulation setup is listed in Tab.I. Firstly, we evaluate the performance of Alg. 1. We limit the reference number within a range of 3 to 20. To assess 3D coordinates, at least 3 references

$$\phi'(N) = \frac{\partial\phi(N)}{\partial d_{2D}} \frac{\partial d_{2D}}{\partial N} = \underbrace{(d_{2D}^2 + h^2)^{\frac{1}{4}\eta} \left[\frac{1}{4} \cdot \eta' \cdot \ln(d_{2D}^2 + h^2) + \frac{2d_{2D}\eta}{d_{2D}^2 + h^2} \right]}_{>0} (d'_{2D}) \quad (23)$$

$$\begin{aligned} \phi''(N) &= \frac{\partial^2\phi(N)}{\partial^2 d_{2D}} \left(\frac{\partial d_{2D}}{\partial N} \right)^2 + \frac{\partial\phi(N)}{\partial d_{2D}} \frac{\partial^2 d_{2D}}{\partial^2 N} \\ &= (d_{2D}^2 + h^2)^{\frac{1}{4}\eta} \left[\underbrace{\frac{\ln(d_{2D}^2 + h^2)}{16} \left((\eta')^2 \ln(d_{2D}^2 + h^2) - \frac{1}{4}\eta'' \right)}_{>0} + \underbrace{\frac{d_{2D}\eta\eta' \ln(d_{2D}^2 + h^2) + 2\eta + 2.5d_{2D}\eta'}{d_{2D}^2 + h^2}}_{>0} \right] (d'_{2D})^2 \\ &\quad + \underbrace{(d_{2D}^2 + h^2)^{\frac{1}{4}\eta} \left[\frac{1}{4}\eta' \cdot \ln(d_{2D}^2 + h^2) + \frac{2d_{2D}\eta}{d_{2D}^2 + h^2} \right]}_{\approx 0} (d''_{2D}) \end{aligned} \quad (24)$$

$$F'_\theta(N) \approx -3N^{-4}\Phi^2(N) + 2N^{-3}\Phi(N)\Phi'(N) = \underbrace{-3N^{-4}\Phi^2(N)}_{<0} + \underbrace{2N^{-3}\Phi(N) \left(\phi(N) + \frac{\phi'(N)}{2} \right)}_{>0} \quad (25)$$

$$\begin{aligned} F''_\theta(N) &= 12N^{-5}\Phi^2(N) - 12N^{-4}\Phi(N)\Phi'(N) + 2N^{-3} \left((\Phi'(N))^2 + \Phi(N)\Phi''(N) \right) \\ &= \underbrace{12N^{-5}\Phi^2(N)}_{>0} - \underbrace{12N^{-4}\Phi(N) \left(\phi(N) + \frac{\phi'(N)}{2} \right)}_{>0} + \underbrace{2N^{-3} \left[\left(\phi(N) + \frac{\phi'(N)}{2} \right)^2 + \Phi(N) \left(\phi'(N) + \frac{\phi''(N)}{2} \right) \right]}_{>0} \end{aligned} \quad (26)$$

TABLE I: Simulation setup 1

	Parameter	Value	Remark
TDOA	f_c	3.5 Ghz	Carrier frequency
	K	(0.1, 3.0)	Rician factors
	N_p	4	Number of multipath
	τ_{\max}	2e-7 s	Maximum delay spread
	P_t	15 dBm	Transmitting power
	N_o	-91 dBm	Noise floor
	β_n	10 Mhz	Bandwidth
	σ_t	1 μ s	Average synchronization error
Deployment	h_u	[20, 30]	UAV altitude
	σ_h	1	Altitude measurement error power
	σ_{GPS}	5	Initial GPS error power
	R	[60, 90, 120]	Node coverage
	h_n	$\sim \mathcal{U}(0, 5)$	Node Altitudes
	Δ_{LOS}	[-0.4, 0.1]	LOS probability modification

are required, while involving too many reference nodes is impractical in practice. Therefore, we limit the reference numbers to 20. The consolidated results of 1000 simulations are presented in Fig. 4.

The simulation results confirm our analytical findings: localization considering node distribution has an optimal solution, and its solution N_{opt} varies with respect to node coverage and altitude. Despite $h_u = 30$ m resulting in generally longer distances to the sensor nodes, the localization performance is still superior due to improved channels. The localization performance when applying Alg. 1 demonstrates a slight

enhancement in localization accuracy and requires fewer reference nodes by providing a dynamic solution to different circumstances. Except for the case where $h_u = 30$ m and $R = 60$ m, the average optimal solution is apparently beyond 20. Under this configuration, Alg. 1 fails to provide comparable performance to $N = 20$. The true N_{opt} is frequently larger than 20. When applying Alg. 1, N_{opt} is bounded by 20, which consequently restricts performance. However, when significantly enlarging N , the performance enhancement is rather limited. Notably, the localization performance in this case is already satisfactory.

It is reasonable to assume that when the UAV precisely knows its altitude and the deployment of ground reference nodes, an empirical optimal solution can be applied for simplicity. However, even neglecting altitude estimation errors and deployment knowledge ambiguity, LOS probability can be heavily impacted by environmental factors, making such empirical solutions infeasible. We therefore modify the P_{los} on top of Eq.(1) and compare the empirical solution with the optimization solution based on Alg.1. The simulation results in Fig. 5 demonstrate that the optimization solution consistently outperforms the empirical solution, particularly under scenarios with poor LOS conditions, showing resilience to LOS variations.

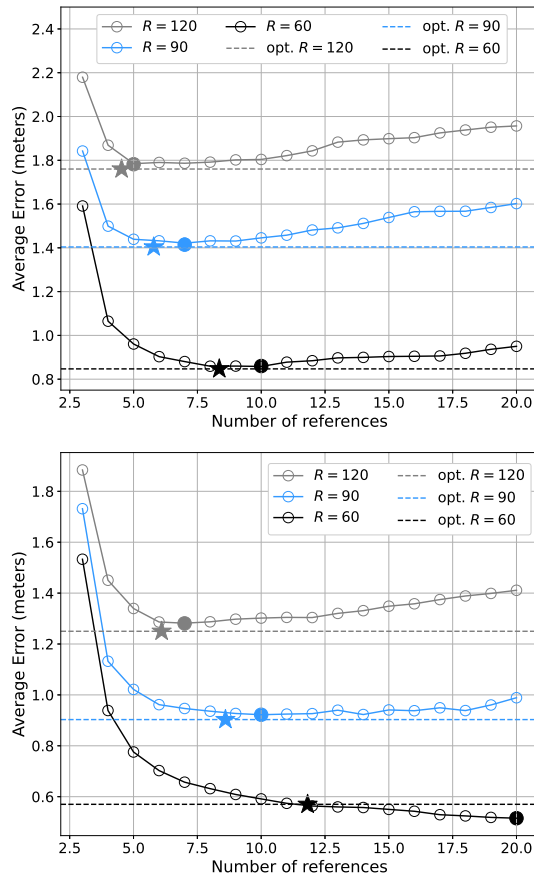


Fig. 4: Localization performance with $h_u = 20$ m (top plot) and $h_u = 30$ m (bottom plot).

VI. CONCLUSION

Our study presents a resource-efficient framework for UAV self-localization by optimizing reference node selection under practical constraints. Simulations validate that the proposed method enhances accuracy while adapting to varying channel conditions. Future work will explore real-world considerations such as unilateral reference problems and dynamic network synchronization for scalable UAV localization in 6G networks.

REFERENCES

- [1] Y. Jiang, X. Li, G. Zhu *et al.*, "Integrated Sensing and Communication for Low Altitude Economy: Opportunities and Challenges," *IEEE Commun. Mag.*, pp. 1–7, 2025.
- [2] M. Khelifi and I. Butun, "Swarm Unmanned Aerial Vehicles (SUAVs): A Comprehensive Analysis of Localization, Recent Aspects, and Future Trends," *Journal of Sensors*, vol. 2022, no. 1, p. 8600674, 2022.
- [3] P. Sinha and I. Guvenc, "Impact of Antenna Pattern on TOA Based 3D UAV Localization Using a Terrestrial Sensor Network," *IEEE Trans. on Veh. Techn.*, vol. 71, no. 7, pp. 7703–7718, 2022.
- [4] Y. Zhao, Z. Li, B. Hao *et al.*, "Sensor Selection for TDOA-Based Localization in Wireless Sensor Networks With Non-Line-of-Sight Condition," *IEEE Trans. on Veh. Techn.*, vol. 68, no. 10, pp. 9935–9950, 2019.
- [5] Y. Zhao, N. Cheng, Z. Li *et al.*, "An efficient sensor selection algorithm for tdoa localization with estimated source position," in *2022 IEEE ICC*, 2022, pp. 871–876.
- [6] Z. Dai, G. Wang, and H. Chen, "Sensor selection for tdoa-based source localization using angle and range information," *IEEE Trans. on Aero. and Ele. Sys.*, vol. 57, no. 4, pp. 2597–2604, 2021.

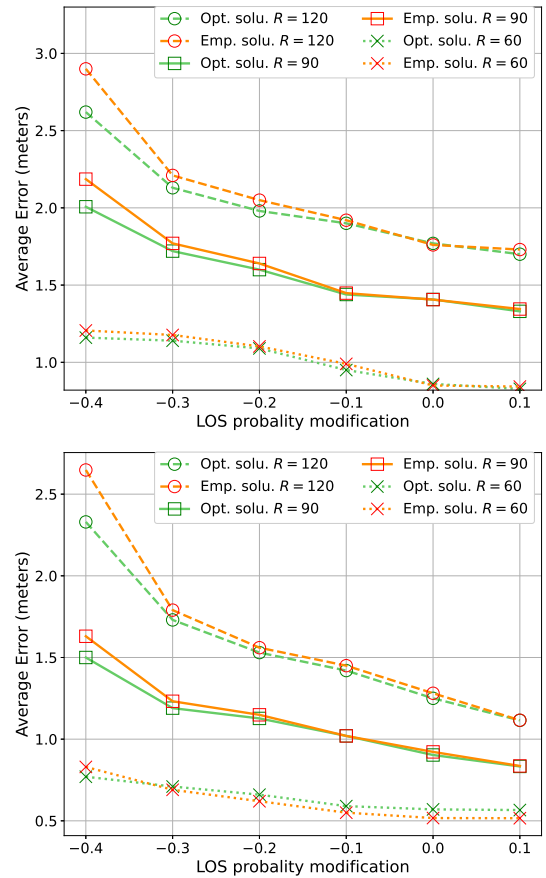


Fig. 5: Localization performance with LOS modification $h_u = 20$ m (top plot) and $h_u = 30$ m (bottom plot).

- [7] S. Kim and J.-W. Chong, "An Efficient TDOA-Based Localization Algorithm without Synchronization between Base Stations," *Inter. Journal of Dist. Sen. Net.*, vol. 11, no. 9, p. 832351, 2015.
- [8] S. Fan, W. Ni, H. Tian *et al.*, "Carrier phase-based synchronization and high-accuracy positioning in 5g new radio cellular networks," *IEEE Trans. on Commun.*, vol. 70, no. 1, pp. 564–577, 2022.
- [9] S. Motie, H. Zayyani, M. Salman *et al.*, "Self uav localization using multiple base stations based on tdoa measurements," *IEEE Wire. Commun. Letters*, vol. 13, no. 9, pp. 2432–2436, 2024.
- [10] 3GPP, "Study on enhanced lte support for aerial vehicles," 3GPP, Tech. Rep. TR 36.777, Dec. 2017, release 15.
- [11] G. F. M. for Digital and Transport. (2021, November) Eu rules for drones. [Online]. Available: <https://dipul.de/homepage/en/aktuelle-meldungen/artikel-3/>
- [12] 3GPP, "Study on channel model for frequencies from 0.5 to 100 GHz," 3GPP, Tech. Rep. TR 38.901, 2020, release 16.
- [13] Y. Zhu, G. Zheng, and M. Fitch, "Secrecy Rate Analysis of UAV-Enabled mmWave Networks Using Matérn Hardcore Point Processes," *IEEE JSAC*, vol. 36, no. 7, pp. 1397–1409, 2018.
- [14] A. Venus, E. Leitinger, S. Tertinek *et al.*, "Reliability and threshold-region performance of toa estimators in dense multipath channels," in *2020 IEEE ICC Workshops*, 2020, pp. 1–7.
- [15] S. Hechenberger, S. Tertinek, and H. Arthaber, "Performance bounds of uwb toa estimation in presence of wi-fi 6e wideband interference," in *2024 14th IPIN*, 2024, pp. 1–6.
- [16] K. Witrals, E. Leitinger, S. Hinteregger *et al.*, "Bandwidth scaling and diversity gain for ranging and positioning in dense multipath channels," *IEEE Wire. Commun. Letters*, vol. 5, no. 4, pp. 396–399, 2016.
- [17] Z. Fang, B. Han, and H. D. Schotten, "Trustworthy UAV Cooperative Localization: Information Analysis of Performance and Security," *IEEE Trans. on Veh. Techn.*, pp. 1–16, 2025.